The Journal of Chemical Physics

Probing structural changes upon carbon monoxide coordination to single metal adatoms

Cite as: J. Chem. Phys. **152**, 051102 (2020); https://doi.org/10.1063/1.5137904
Submitted: 14 November 2019 • Accepted: 08 January 2020 • Published Online: 04 February 2020

P. T. P. Ryan, M. Meier, Z. Jakub, et al.

The Journal of Chemical Physics COMMUNICATION scitation.org/journal/jcp

Probing structural changes upon carbon monoxide coordination to single metal adatoms

Cite as: J. Chem. Phys. 152, 051102 (2020); doi: 10.1063/1.5137904
Submitted: 14 November 2019 • Accepted: 8 January 2020 •
Published Online: 4 February 2020

P. T. P. Ryan,[1,2] M. Meier,[3,4] Z. Jakub,[3] J. Balajka,[4] J. Hulva,[3] D. J. Payne,[2] T.-L. Lee,[1] C. Franchini,[4] F. Allegretti,[5] G. S. Parkinson,[3] and D. A. Duncan[1,a)]

AFFILIATIONS

[1]Diamond Light Source, Harwell Science and Innovation Campus, Didcot OX11 0QX, United Kingdom
[2]Department of Materials, Imperial College London, London SW7 2AZ, United Kingdom
[3]Institute of Applied Physics, TU Wien, 1040 Vienna, Austria
[4]University of Vienna, Faculty of Physics and Center for Computational Materials Science, 1090 Vienna, Austria
[5]Physics Department E20, Technical University of Munich, 85748 Garching, Germany

Note: This article is part of the JCP Special Topic on Oxide Chemistry and Catalysis.
[a)]**Author to whom correspondence should be addressed:** David.duncan@diamond.ac.uk

ABSTRACT

In this work, the adsorption height of Ag adatoms on the $Fe_3O_4(001)$ surface after exposure to CO was determined using normal incidence x-ray standing waves. The Ag adatoms bound to CO (Ag_1^{CO}) are found to be pulled out of the surface to an adsorption height of 1.15 Å ± 0.08 Å, compared to the previously measured height of 0.96 Å ± 0.03 Å for bare Ag adatoms and clusters. Utilizing DFT+vdW+U calculations with the substrate unit cell dimension fixed to the experimental value, the predicted adsorption height for Ag_1^{CO} was 1.16 Å, in remarkably good agreement with the experimental results.

I. INTRODUCTION

A recent drive in the field of heterogeneous catalysis is the complete dispersion of the catalytically active metal into isolated centers, so called single atom catalysts (SACs). The motivation for atomic dispersion is not only the improved economics associated with the more efficient utilization of often expensive and rare metals but also the improved control over the properties of the resulting catalytic material such as catalyst activity[1–4] and catalyst selectivity,[5–7] catalytic properties more generally associated with homogeneous catalysis. SACs have also been used to tackle the poisoning of heterogeneous catalysts [e.g., the use of an atomically dispersed Pt single atom alloy (SAA)].[8] However, development of such SACs is highly reliant on accurate density functional theory (DFT) calculations for predicting reaction mechanisms to understand measured catalytic activity and for improving the screening of new catalytic materials.[2,9–13] Yet, these DFT calculations can only be validated by comparison to quantitative experiments. Specifically, the geometric structure of an adsorbate is an important bellwether of the accuracy of such calculations, as it is intrinsically linked to both the electronic structure of the system and the potential reaction mechanisms and pathways that are sterically available.

In addition to potential direct industrial applications, SACs provide model catalytic materials with which thorough studies of catalyst functionality can be undertaken; many SAC systems rely on a crystalline substrate, e.g., a metal or metal-oxide surface, with well-defined repeating adsorption sites onto or into which the isolated metal centers are stabilized.[5,8,14–19] An interesting consequence of the isolated nature of the active metal centers in SAC systems is the parallels that can be drawn between SAC systems and metal organic

complexes used in homogeneous catalysis.[20] An example of such a study is a recently published article by Jakub *et al.*[21] who investigated the coordination geometries of Ir carbonyls on the subsurface cation vacancy (SCV) reconstruction[22] of the $Fe_3O_4(001)$ surface, a reconstruction well known to stabilize a range of different metal adatom phases.[19,21–26] The study showed that Ir dicarbonyl complexes on the $Fe_3O_4(001)$ surface were found in a square planar geometry, the preferred geometry of Ir(I) d^8 electron complexes.[27] More generally, there is interest in understanding the interaction of CO with these SAC systems, specifically, how it modifies the material's morphology and structure, which can have far reaching effects on its catalytic properties. Such studies have included investigations of Pt and Pd adatoms on the same SCV reconstruction where adsorption of CO resulted in gas sintering of the adatoms into subnanometer Pt and Pd clusters.[23,24] However, to date, no quantitative structural studies into these systems have been pursued.

In our prior work, we used the normal incidence x-ray standing wave (NIXSW) technique to probe the adsorption geometry of Ag and Cu adatoms without prior exposure to any additional ligands (Ag_1^{bare} and Cu_1^{bare}, respectively) on the $Fe_3O_4(001)$ SCV reconstruction,[25] as well as the incorporation of Ni_1^{bare} adatoms.[26] For all three metal species investigated, the adatoms (prior to incorporation) were determined to be in the bulk continuation tetrahedral sites bound to two surface oxygen atoms, with each metal adatom sitting at a different height relative to the surface Fe_{oct} layer (0.96 Å ± 0.03 Å for Ag_1^{bare}, 0.43 Å ± 0.03 Å for Cu_1^{bare}, and 0.46 Å ± 0.17 Å for Ni_1^{bare}). The complementary DFT calculations found that the commonly used Perdew–Burke–Ernzerhof+U (PBE+U) and PBEsol+U approaches performed poorly when allowed to relax the dimensions of the substrate unit cell, especially when modeling the Ag_1^{bare} adatom. This, in turn, raises questions over the validity of the DFT calculations that underpin much of the work into SACs on strongly interacting oxide supports.[2,9–12] While the Heyd–Scuseria–Ernzerhof (HSE) hybrid functional reproduced the absolute adsorption height of the Ag_1^{bare} and Cu_1^{bare} adatoms well, such functionals are computationally expensive. However, by forcing the PBE+U calculations to utilize the experimental dimensions of the substrate unit cell, the predicted adsorption heights of both the Ag_1^{bare} and Cu_1^{bare} adatoms better represented experimental measurements. Here, we further test this PBE+U approximation by comparing it against a similar NIXSW study of CO on $Ag/Fe_3O_4(001)$ in order to probe whether this methodology can also predict the structure after the ligation to a simple molecule.

II. METHOD

A. Sample preparation

The SCV reconstruction of the $Fe_3O_4(001)$ surface was prepared by conventional UHV sputtering and annealing procedures. Low energy electron diffraction (LEED) and soft x-ray photoelectron spectroscopy (SXPS) of the prepared surface were undertaken to ensure that the $Fe_3O_4(001)$ SCV reconstruction had properly formed.[22] An Omicron EFM3 evaporator was used to deposit 0.4 ML of Ag on the prepared SCV surface at room temperature. The Ag deposition rate was monitored using a quartz crystal microbalance (QCM), which was placed in front of the sample in approximately the position that the sample would occupy during deposition. The rate on the QCM was observed until the desired evaporation rate was stable over a period of a few minutes, before depositing the Ag metal onto the surface. CO was exposed to the sample, which was held at 150 K, by back filling a chamber through a high precision leak valve. Two exposures were undertaken, specifically, exposing the $Ag/Fe_3O_4(001)$ to 10 L or 20 L of CO, where 1 L corresponds to 10^{-6} mbar·s. Note the CO exposures were undertaken with the same prepared Ag/Fe_3O_4 surface used to measure the NIXSW of our previous Ag/Fe_3O_4 study.

B. Experimental method

The NIXSW technique[28] relies upon the creation of an x-ray standing wave when the Bragg condition is satisfied for a crystal. The x-ray standing wave is produced by the interference between the incident and reflected photon beams, and its periodicity is equal to that of the real space distance (d-spacing) that corresponds to the substrate Bragg planes. As outlined in dynamical diffraction studies of the creation of the standing wave,[29] the phase of the x-ray standing wave relative to the d-spacing changes by π when the energy of the incident photon beam is scanned through the Bragg condition. Therefore, the x-ray intensity experienced by an atom, and in turn the x-ray photoelectron yield, during the photon energy scan will be characteristic of the location of the atom relative to the d-spacing. Modeling these photoelectron yield profiles using dynamical diffraction theory yields two dimensionless fitting parameters:[28] the coherent fraction, f^{hkl}, and the coherent position, P^{hkl}. If the emitter is located at one ordered adsorption site in the given direction, the latter parameter can be interpreted as the position the emitter takes along the d-spacing of the chosen reflection, taking values in the range 0–1. The former can be interpreted as the level of order of the emitter and is related to the distribution of positions that the emitters occupy within the d-spacing.[30] For all the dynamical diffraction calculations of the reflection intensity undertaken here, the Fe_3O_4 unit cell was centered on a Fe_{tet} atom and, as such, coherent positions of 0 or 1 in the (004) direction are defined as being coincident with the Fe_{tet} layers. In this work, the photon energy was scanned around an energy of 2.955 keV [the energy of the (004) reflection of the bulk Fe_3O_4 crystal after cooling to 150 K] and photoelectron yield profiles from the Ag $3d_{5/2}$ core-level were acquired as a function of the photon energy.

C. Computational details

The Vienna *ab initio* simulation package (VASP)[31,32] was used for all DFT calculations using the optB88-DF[33–36] van der Waals functional with an effective on-site Coulomb repulsion term U_{eff} = 3.61 eV. The Projector Augmented Wave (PAW) method[37,38] describes the electron-ion interactions. The plane wave basis set cutoff energy was set to 550 eV. An asymmetric slab with 13 planes (5 fixed and 2 relaxed Fe_{oct} laers) and 14 Å vacuum was used. To avoid interaction between adsorbates and to accurately model the experimental coverages, a (2 × 2) supercell was used [i.e., four times the $(\sqrt{2} \times \sqrt{2})R45^\circ$ reconstructed cell] with a lattice constant of 16.794 Å [corresponding to a (1 × 1) lattice constant of 8.397 Å]. These supercell calculations have been performed at the Γ-point only. Fixing the lattice constant at the experimental value would be

expected to result in alterations to the surface free energy and the density of states, yet the predicted surface free energy diagram is unchanged with respect to that published previously with a relaxed lattice constant,[22] and these calculations also predict an insulating surface layer, as is expected.

III. RESULTS AND DISCUSSION

The hard X-ray photoelectron spectroscopy (HAXPES) spectra of the Ag 3*d* core level for the as deposited Ag (Ag^{bare}) and after exposure to 10 L/20 L of CO (Ag^{CO}) are shown in Fig. 1. The Ag^{bare} spectrum and the corresponding photoelectron yield profiles are already published and are reproduced here for comparison.[25] Note that the exposure of CO was undertaken with the same prepared Ag/Fe_3O_4 surface as the previously published Ag^{bare} data. The Ag^{bare} spectrum was fitted with a single, somewhat broad, peak and, in our previous work, assigned to a mixture of Ag adatoms on the surface (Ag_1^{bare}) and a small number of Ag clusters present on the surface ($Ag_{clusters}^{bare}$). Due to the variations in the line shape observed while scanning the photon energy in the NIXSW data, the Ag^{CO} spectra were fitted with two narrower peaks (Ag_{low}^{CO} and Ag_{high}^{CO} at lower and higher binding energy, respectively). Note that the Ag_{low}^{CO} relative intensity increases with higher CO exposure and is assigned to a mixture of clusters of Ag adatoms with CO ($Ag_{clusters}^{CO}$), as well as any remaining Ag_1^{bare} adatoms and $Ag_{clusters}^{bare}$. Ag_{high}^{CO}, with a binding energy shift of 0.6 eV with respect to Ag^{bare}, comparable to the 0.7 eV shift found for CO exposure to Ir,[21] was assigned to Ag adatoms coordinated to CO molecules (Ag_1^{CO} in the following). Note that in order to improve data quality, the 20 L spectra were acquired with a higher analyzer pass energy (500 eV vs 200 eV).

The corresponding, fitted, (004) photoelectron yield profiles for the Ag^{bare} (taken from Ref. 25), Ag_{low}^{CO}, and Ag_{high}^{CO} species after the 20 l CO exposure are shown in Fig. 2(a), and the resulting coherent fractions, coherent positions, and real space heights (D_{exp}^{004}) above the bulk-terminated Fe_{oct} layer are listed in Table I. The photoelectron yield profiles and values for the 10 L CO exposure can be found in Fig. S1 and Table S1 in the supplementary material and agree well with those after the 20 L exposure. Note that a lower coherent fraction is observed for the (044) and (113) reflections: the former is

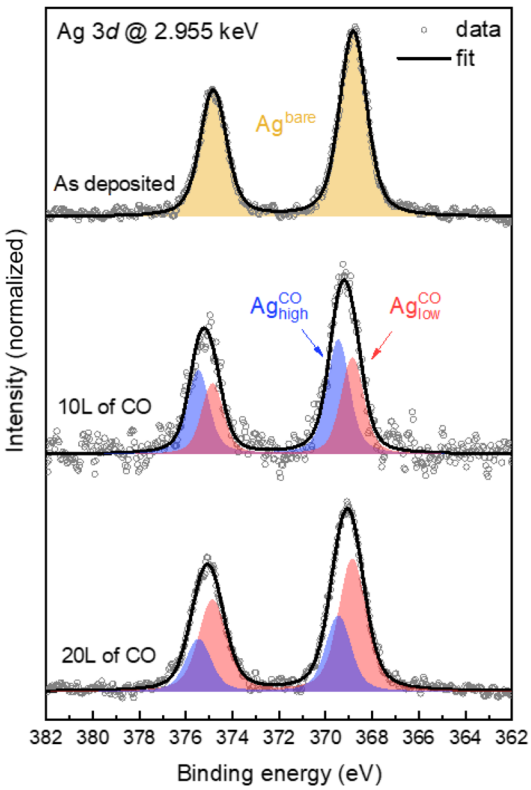

FIG. 1. Peak fitted Ag 3d HAXPES spectra, integrated over multiple repeated measurements on different spots on the sample, for the as deposited 0.4 ML of Ag [Reproduced with permission from Meier *et al.*, Nanoscale **10**, 2226 (2018). Copyright 2018 The Royal Society of Chemistry] and after exposure to 10 L and 20 L of CO.

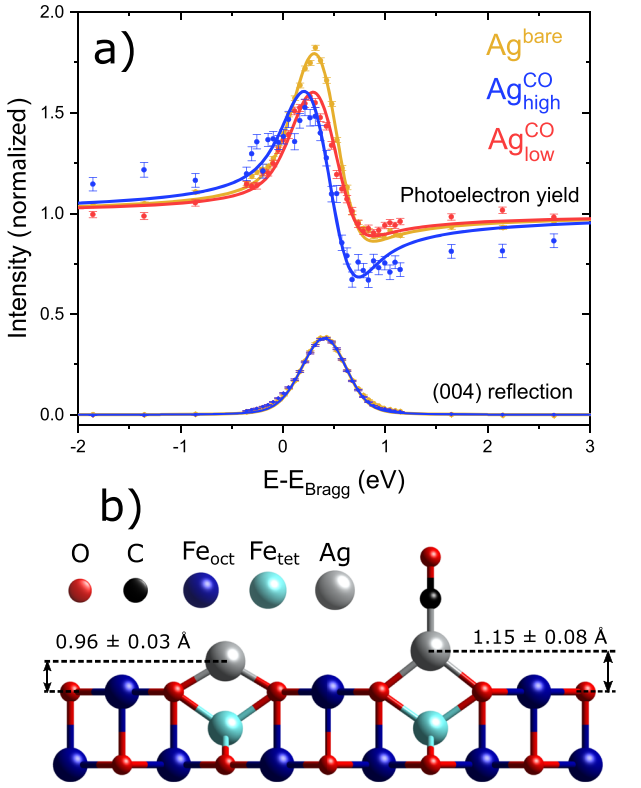

FIG. 2. (a) The (004) reflection for the Fe_3O_4 crystal as well as the fitted NIXSW photoelectron yield profiles, integrated over multiple repeated measurements on different spots on the sample, for the deposited 0.4 ML of Ag (Ag^{bare}) [Reproduced with permission from Meier *et al.*, Nanoscale **10**, 2226 (2018). Copyright 2018 The Royal Society of Chemistry] and for the two Ag photoemission features after exposure of the Ag^{bare} surface to 20 L of CO (Ag_{low}^{CO} and Ag_{high}^{CO}). (b) The resulting adsorption heights above a bulk terminated surface are shown schematically for the Ag^{bare} and Ag_{high}^{CO} species, assuming a single adsorption height.

TABLE I. Measured coherent fractions (f^{004}), coherent positions (P^{004}), and adsorption heights above a projected bulk Fe_{oct} surface layer (D^{004}_{exp}) for Ag^{bare} [a], Ag^{CO}_{low}, and Ag^{CO}_{high}, shown in Fig. 2, compared against the theoretically calculated adsorption height above a projected bulk Fe_{oct} surface layer (D^{004}_{DFT}) for the Ag^{bare}_1 and Ag^{CO}_1 adatoms.

	f^{004} [b]	P^{004} [b]	D^{004}_{exp} (Å) [b]	D^{004}_{DFT} (Å)
Ag^{bare} [a]	0.66(3)	0.96(1)	0.96(3)	(Ag^{bare}_1) 0.87
Ag^{CO}_{high}	0.89(9)	0.05(4)	1.15(8)	(Ag^{CO}_1) 1.16
Ag^{CO}_{low}	0.47(4)	0.00(2)	1.05(4)	...

[a]Note that the Ag^{bare} data are taken from our previously published work.[25]
[b]The values in brackets are the errors in the last significant figure.

due to the inability to separate the Ag^{CO}_{low} and Ag^{CO}_{high} components at the higher photon energy used for the (044) reflection, and the latter is due to the point group symmetry of the surface that results in the identical surface tetrahedral sites having differing coherent positions with respect to the (113) x-ray standing wave. The NIXSW data identify that the coordination of CO to the Ag^{bare}_1 adatoms, forming Ag^{CO}_1 adatoms, results in an increase in adsorption height to 1.15 Å ± 0.08 Å. A significant increase in the coherent fraction is also observed. Moreover, we have determined that the adsorption of CO does not alter the lateral registry of the Ag^{CO}_1 adatom (Fig. S2). The coherent fraction of the Ag^{CO}_{low} feature has, in contrast, decreased significantly compared to the Ag^{bare} and Ag^{CO}_{high} results. This lower coherent fraction suggests that this feature does indeed, at least partially, correspond to the clusters of Ag atoms, which will occupy multiple adsorption sites with respect to the lattice planes that define the x-ray standing wave. The increased intensity of Ag^{CO}_{low} with greater CO exposures might suggest that CO is inducing greater clustering, an effect that has been observed for other metal adatoms on magnetite at room temperature,[23,24] although no such effect has been observed by STM at 150 K for Ag. This apparent increase in clustering of the Ag atoms on the surface could also be due to a difference in the Ag coverage of the two preparations. However, to explain such a stark difference between the 10 L and 20 L preparations would require an ~50% increase in the Ag coverage, which would not be consistent with the monitoring of the evaporation rate by using the QCM.

As there is an overlap in binding energy between Ag^{bare}_1, $Ag^{bare}_{clusters}$, and $Ag^{CO}_{clusters}$, we cannot individually separate the coherent fractions and positions of these three components nor can we identify relative coverages. Therefore, the measured f^{004} and P^{004} of Ag^{bare} are a combination of the respective coherent fractions and positions of Ag^{bare}_1 and $Ag^{bare}_{clusters}$; the measured f^{004} and P^{004} of Ag^{CO}_{low} are a combination of the respective coherent fractions and positions of Ag^{bare}_1, $Ag^{bare}_{clusters}$, and $Ag^{CO}_{clusters}$. We can assume that the coherent fraction of the Ag^{bare}_1 adatoms should be as high as the coherent fraction of the Ag^{CO}_1 (Ag^{CO}_{high}) adatoms and that the relative coverage of Ag^{bare}_1, with respect to the combined coverage of $Ag^{bare}_{clusters}$ and $Ag^{CO}_{clusters}$, decreases after CO exposure. We also know that after exposure to 10 L of CO, the coverage of Ag^{CO}_{high} is greater than the combined coverage of all three other species, and thus, the majority, if not all, of Ag^{bare}_1 have been converted to either Ag^{CO}_1 or one of the two cluster species. Finally, the coherent position of Ag^{CO}_{low} is not equal to that of Ag^{bare}. The consequence of this is that the measured coherent fraction for Ag^{CO}_{low} cannot be reconciled with $f^{004}_{Ag^{CO}_{clusters}}$ and $f^{004}_{Ag^{bare}_{clusters}}$ both being zero; at least one, if not both, must be non-zero.

In our prior work, we assumed that $f^{004}_{Ag^{bare}_{clusters}}$ was zero, and thus, the presence of $Ag^{bare}_{clusters}$ would have no effect on the measured coherent position for $P^{004}_{Ag^{bare}_1}$. This work suggests that the assumption could be false, although it may be that $f^{004}_{Ag^{bare}_{clusters}}$ is zero and $f^{004}_{Ag^{CO}_{clusters}}$ non-zero. As the measured $D^{004}_{Ag^{CO}_{low}}$ is slightly higher than that of $D^{004}_{Ag^{bare}}$ by 0.09 Å ± 0.05 Å, the actual adsorption height of Ag^{bare}_1 could well be less than 0.96 Å ± 0.01 Å. How much less is impossible to say, but it is worth noting that in our prior calculations and those presented here, Ag^{bare}_1 was predicted to have an adsorption height of 0.87 Å, i.e., ~0.10 Å lower than the measured Ag^{bare} height. Thus, the theoretical calculations utilizing either the HSE functional or the PBE+U functional with the Fe_3O_4 unit cell fixed at the experimental values may be more accurate than we had assumed in our prior work. Moreover, performing these calculations for the Ag^{CO}_1 adatom results in a predicted adsorption height of 1.16 Å, in almost perfect agreement with the experimental results. The excellent agreement with the experimental results of this DFT approach may lead to computationally affordable and accurate theoretical predictions of not only the single atom catalyst structure but also predictions of molecular adsorption energies and electronic structure, properties that are of paramount importance for theoretical screening of new and improved single atom catalytic materials.

IV. CONCLUSIONS

In this work, we present the first quantitative study of the effects of CO ligation to a single metal adatom dispersed on a supporting substrate. We demonstrate that the CO molecule pulls the silver adatom out of the Fe_3O_4(001) surface by 0.19 Å ± 0.08 Å, compared to the value measured for a mixture of uncoordinated Ag^{bare}_1 adatoms and Ag nanoclusters, to an adsorption height of 1.15 Å ± 0.08 Å above a projected bulk like Fe_{oct} termination. As the coordination of CO to a metal center is an important intermediate state in many reactions (e.g., CO oxidation, water gas shift, CO_2 reformation, and syngas production) and a common poison in many other catalytic reactions, understanding how the metal center is altered by this coordination is an important step in being able to understand reaction mechanisms and pathways.

Our prior study into Ag^{bare}_1 and Cu^{bare}_1 adatoms on the same surface proposed a methodology for overcoming the failure of PBE+U calculations in predicting the adsorption height of such species—by pinning the Fe_3O_4 unit cell dimensions to experimental values (8.397 Å). Performing such calculations for a Ag^{CO}_1 adatom coordinated to CO results in a predicted adsorption height of 1.16 Å, above a projected bulk like Fe_{oct} termination, in perfect agreement with the experimental results. As CO coordination is often used

as a model intermediate state, it is an important benchmark for calculations aimed at modeling catalytic reactions. The excellent agreement presented here suggests that this methodology could well be applicable to modeling the catalytic activity of these adatoms toward a wide variety of chemical reactions. Further study, however, is required in order to elucidate its potential to model such activity and understand the limitations of this methodology. Thus, in this work, we further justify this approach for performing computationally affordable, but highly accurate DFT calculations for the reactivity of metal adatoms on the magnetite surface.

SUPPLEMENTARY MATERIAL

See the supplementary material for a description of the real space imaging, (Fig. S1) the (113) and (044) NIXSW data for Ag^{CO}_{high} and Ag^{CO}_{low}, (Fig. S2) the real space imaging for Ag^{CO}_{high}, (Fig. S3) the (004) NIXSW data after a 10 L exposure to CO, and (Table S1) the measured coherent fractions and positions for the three different reflections.

ACKNOWLEDGMENTS

The authors gratefully acknowledge funding through projects from the Austrian Science Fund FWF (Grant No. start-Prize Y 847-N20) (M.M., J.H. and G.S.P) and the Doctoral College TU-D (Z.J.); the. P.T.P.R. would like to thank the Advanced Characterisation of Materials (ACM) CDT. The computational results were achieved in part using the Vienna Scientific Cluster (VSC 3). F.A. acknowledges support by Deutsche Forschungsgemeinschaft (DFG) through TUM International Graduate School of Science and Engineering (IGSSE). We also thank Diamond Light Source for the award of beam time (No. SI13817-1).

REFERENCES

[1] J. Lin, A. Wang, B. Qiao, X. Liu, X. Yang, X. Wang, J. Liang, J. Li, J. Liu, and T. Zhang, J. Am. Chem. Soc. **135**, 15314 (2013).
[2] B. Qiao, A. Wang, X. Yang, L. F. Allard, Z. Jiang, Y. Cui, J. Liu, J. Li, and T. Zhang, Nat. Chem. **3**, 634 (2011).
[3] T. Kropp, Z. Lu, Z. Li, Y. H. C. Chin, and M. Mavrikakis, ACS Catal. **9**, 1595 (2019).
[4] X. F. Yang, A. Wang, B. Qiao, J. Li, J. Liu, and T. Zhang, Acc. Chem. Res. **46**, 1740 (2013).
[5] F. R. Lucci, J. Liu, M. D. Marcinkowski, M. Yang, L. F. Allard, M. Flytzani-Stephanopoulos, and E. C. H. Sykes, Nat. Commun. **6**, 8550 (2015).
[6] Y. Dong, W. Li, Z. Yan, and J. Zhang, Catal. Sci. Technol. **6**, 7946 (2016).
[7] H. Wei, X. Liu, A. Wang, L. Zhang, B. Qiao, X. Yang, Y. Huang, S. Miao, J. Liu, and T. Zhang, Nat. Commun. **5**, 5634 (2014).
[8] J. Liu, F. R. Lucci, M. Yang, S. Lee, M. D. Marcinkowski, A. J. Therrien, C. T. Williams, E. C. H. Sykes, and M. Flytzani-Stephanopoulos, J. Am. Chem. Soc. **138**, 6396 (2016).
[9] J. X. Liang, X. F. Yang, A. Wang, T. Zhang, and J. Li, Catal. Sci. Technol. **6**, 6886 (2016).
[10] J. X. Liang, J. Lin, X. F. Yang, A. Q. Wang, B. T. Qiao, J. Liu, T. Zhang, and J. Li, J. Phys. Chem. C **118**, 21945 (2014).
[11] Y. Tang, Y. G. Wang, and J. Li, J. Phys. Chem. C **121**, 11281 (2017).
[12] F. Li, Y. Li, X. C. Zeng, and Z. Chen, ACS Catal. **5**, 544 (2015).
[13] C. K. Narula, L. F. Allard, G. M. Stocks, and M. Moses-Debusk, Sci. Rep. **4**, 7238 (2014).
[14] G. X. Pei, X. Y. Liu, A. Wang, A. F. Lee, M. A. Isaacs, L. Li, X. Pan, X. Yang, X. Wang, Z. Tai, K. Wilson, and T. Zhang, ACS Catal. **5**, 3717 (2015).
[15] B. Yang, X. Lin, H. J. Gao, N. Nilius, and H. J. Freund, J. Phys. Chem. C **114**, 8997 (2010).
[16] A. S. Hoffman, L. M. Debefve, S. Zhang, J. E. Perez-Aguilar, E. T. Conley, K. R. Justl, I. Arslan, D. A. Dixon, and B. C. Gates, ACS Catal. **8**, 3489 (2018).
[17] H. V. Thang, S. Tosoni, L. Fang, P. Bruijnincx, and G. Pacchioni, ChemCatChem **10**, 2634 (2018).
[18] H. V. Thang, G. Pacchioni, L. DeRita, and P. Christopher, J. Catal. **367**, 104 (2018).
[19] Z. Novotný, G. Argentero, Z. Wang, M. Schmid, U. Diebold, and G. S. Parkinson, Phys. Rev. Lett. **108**, 216103 (2012).
[20] X. Cui, W. Li, P. Ryabchuk, K. Junge, and M. Beller, Nat. Catal. **1**, 385 (2018).
[21] Z. Jakub, J. Hulva, M. Meier, R. Bliem, F. Kraushofer, M. Setvin, M. Schmid, U. Diebold, C. Franchini, and G. S. Parkinson, Angew. Chem., Int. Ed. **58**, 13961 (2019).
[22] R. Bliem, E. McDermott, P. Ferstl, M. Setvin, O. Gamba, J. Pavelec, M. A. Schneider, M. Schmid, U. Diebold, P. Blaha, L. Hammer, and G. S. Parkinson, Science **346**, 1215 (2014).
[23] R. Bliem, J. E. S. van der Hoeven, J. Hulva, J. Pavelec, O. Gamba, P. E. de Jongh, M. Schmid, P. Blaha, U. Diebold, and G. S. Parkinson, Proc. Natl. Acad. Sci. U. S. A. **113**, 8921 (2016).
[24] G. S. Parkinson, Z. Novotny, G. Argentero, M. Schmid, J. Pavelec, R. Kosak, P. Blaha, and U. Diebold, Nat. Mater. **12**, 724 (2013).
[25] M. Meier, Z. Jakub, J. Balajka, J. Hulva, R. Bliem, P. K. Thakur, T. L. Lee, C. Franchini, M. Schmid, U. Diebold, F. Allegretti, D. A. Duncan, and G. S. Parkinson, Nanoscale **10**, 2226 (2018).
[26] P. T. P. Ryan, Z. Jakub, J. Balajka, J. Hulva, M. Meier, J. T. Küchle, P. J. Blowey, P. K. Thakur, C. Franchini, D. J. Payne, D. P. Woodruff, L. A. Rochford, F. Allegretti, T. L. Lee, G. S. Parkinson, and D. A. Duncan, Phys. Chem. Chem. Phys. **20**, 16469 (2018).
[27] J. P. Collman, Acc. Chem. Res. **1**, 136 (1968).
[28] D. P. Woodruff, Rep. Prog. Phys. **68**, 743 (2005).
[29] B. W. Batterman, Phys. Rev. **133**, A759 (1964).
[30] D. P. Woodruff, Prog. Surf. Sci. **57**, 1 (1998).
[31] G. Kresse and J. Furthmüller, Comput. Mater. Sci. **6**, 15 (1996).
[32] G. Kresse and J. Hafner, Phys. Rev. B **48**, 13115 (1993).
[33] M. Dion, H. Rydberg, E. Schröder, D. C. Langreth, and B. I. Lundqvist, Phys. Rev. Lett. **92**, 246401 (2004).
[34] J. Klimeš, D. R. Bowler, and A. Michaelides, J. Phys. Condens. Matter **22**, 022201 (2010).
[35] K. Lee, É. D. Murray, L. Kong, B. I. Lundqvist, and D. C. Langreth, Phys. Rev. B **82**, 081101 (2010).
[36] G. Román-Pérez and J. M. Soler, Phys. Rev. Lett. **103**, 096102 (2009).
[37] P. E. Blöchl, Phys. Rev. B **50**, 17953 (1994).
[38] D. Joubert, Phys. Rev. B **59**, 1758 (1999).